HiSST: 3rd International Conference on
High-Speed Vehicle Science Technology
14 -19 April 2024, Busan, Korea

# Preliminary Conceptual Design of the Reusable Unmanned Space Vehicles using Multidisciplinary Optimization

*Dabeen Jeong[1], Shinkyu Jeong[2], Jongho Jung[3]*

## Abstract

This study investigates the optimization of a reusable unmanned space vehicle with various objective functions: weight and heat flux minimization. Multi-Objective Genetic Algorithm (MOGA) was used to optimize various objective functions. To compute the objective functions, aerodynamic and thermal analysis was performed during the re-entry process. The modified Newtonian flow and the approximate convective-heating equation were used for aerothermodynamic analysis. After the thermal analysis was performed, the wall temperature was calculated for designing the Thermal Protection System (TPS) layout. Optimization was computed with KSP-1 provided by the Korea Aerospace Research Institute (KARI) was used as a baseline configuration. According to the comparison geometry-based TPS layout and wall temperature-based TPS layout, the wall temperature-based TPS layout was generally lower in weight and protected high-temperature areas that the geometry-based TPS layout did not capture.

**Keywords**: *Reusable Unmanned Space Vehicle, Aerothermodynamic, Multi-Objective Genetic Algorithm, Thermal Protection Systems Layout*

## Nomenclature

Greek

$\gamma$ – Ratio of specific heat

$\rho$ – Density

$\mu$ – Viscosity

$\theta$ - Angle

$\Theta$ – Momentum thickness

Latin

h – Enthalpy

V – Velocity

u – Velocity of x-direction component

$C_p$ – Pressure coefficient

Pr – Prandtl number

Re – Reynolds number

Superscripts

* - Eckert's Reference value

Subscripts

L - Laminar

e - Edge

stag – Stagnation point

aw – Adiabatic wall

w – Wall

$\infty$ - Free stream

## 1. Introduction

Currently, a growing number of projects have been focused on the development of reusable space vehicles, regardless of government and companies. Korea government is also actively participating in

[1] *Kyung Hee University, Department of Mechanical Engineering, Yong-In, Korea, manybeans@khu.ac.kr*
[2] *Kyung Hee University, Department of Mechanical Engineering, Yong-in, Korea, icarus@khu.ac.kr*
[3] *Seoul National University, Department of Aerospace Engineering, Seoul, Korea, jjhjjh01@snu.ac.kr*

reusable space vehicle research, starting with the establishment of the Reusable Unmanned Space Vehicle Research Center in 2022. To consider the reusability of space vehicles, the re-entry process in space needs to be researched. In this study, multidisciplinary optimization was conducted to optimize the reusable unmanned space vehicle under the re-entry process. When a space vehicle re-enters Earth's atmosphere from space, it does so at an exceedingly high velocity, reaching peak speeds of approximately Mach 30, and the friction between the atmosphere and the vehicle's surface generates intense heat [1]. Within the hypersonic regime, obtaining experimental data is significantly challenging, especially when dealing with full-scale models. Therefore, the analysis of the hypersonic region predominantly relies on computational resources. There are various methodologies for analysis in the hypersonic region, such as the Reynolds Average Navier-Stokes (RANS) [2] and the Newtonian Method flow [3]. RANS, being based on the Navier-Stokes (NS) equations, is relatively accurate but demands substantial computing resources. Analyzing the re-entry process requires consideration of the changing altitude as the vehicle descends. For accurate analysis, these altitude changes must occur in small time steps. However, using RANS for altitude-by-altitude analysis becomes computationally intensive and time-consuming. To mitigate the computational resources, the Modified-Newtonian flow and an approximate convective-heating equation are used for hypersonic aerothermodynamics analysis [3-4]. Furthermore, for achieving optimal designs involving various objective functions, a Multi-Optimization Genetic Algorithm (MOGA) is used to optimize the vehicle [5]. In the previous research by Jong Ho et al, the Thermal Protection System (TPS) layout was based on the geometry, the nose and leading edge were coated with reinforced carbon-carbon (RCC), the lower surface of the fuselage and wing were coated with high-temperature reusable surface insulation (HRSI), and other areas were coated with fibrous refractory composite insulation (FRSI) [6]. However, due to the sensitivity of TPS layout to temperature, geometry-based TPS layout can cause problems for the spacecraft's safety. Therefore, the TPS layout was conducted by calculating the wall temperature based on the computed heat flux.

## 2. Methodology

### 2.1. Geometry Design and Weight Analysis

To determine the geometry, 22 parameters were used to define the fuselage, wing planform, airfoil, and winglets. The nose section of the fuselage was created with a spherically blunted tangent ogive curve with rectangular height with corner radius. The airfoil was defined as NACA 4-digit series. Fig. 1 and Table 1 provide the data corresponding to each parameter. After defining the geometry, Hypersonic Aerospace Sizing Analysis (HASA) was employed for weight analysis of the geometry[7].

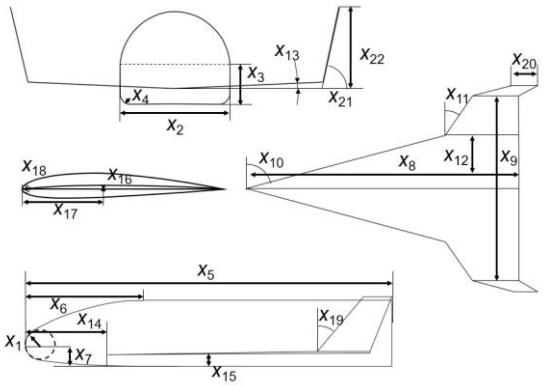


**Fig 1.** Geometry Design parameters

**Table 1.** Geometry Design Parameters

| Part | Design parameter | Description |
|---|---|---|
| **Fuselage** | $X_1$ | Nose radius [m] |
| | $X_2$ | Fuselage width [m] |
| | $X_3$ | Rectangular height [m] |
| | $X_4$ | Corner radius of fuselage section (radius / (width / 2)) [ ] |
| | $X_5$ | Total length [m] |
| | $X_6$ | Nose length (nose length / total length) [ ] |
| | $X_7$ | Nose height [m] |
| **Wing** | $X_8$ | Root chord length [m] |
| | $X_9$ | Span [m] |
| | $X_{10}$ | 1st sweep angle [°] |
| | $X_{11}$ | 2nd sweep angle [°] |
| | $X_{12}$ | Kink position (kink position / span) [ ] |
| | $X_{13}$ | Dihedral angle [°] |
| | $X_{14}$ | Wing longitudinal position (position / total length) [ ] |
| | $X_{15}$ | Wing vertical position (position / total height) [ ] |
| **Airfoil** | $X_{16}$ | Camber [ ] |
| | $X_{17}$ | Camber position [ ] |
| | $X_{18}$ | Leading edge radius [m] |
| **Winglet** | $X_{19}$ | Sweep angle [°] |
| | $X_{20}$ | Tip chord length [m] |
| | $X_{21}$ | Dihedral angle [°] |
| | $X_{22}$ | Span [m] |

### 2.2. Aerodynamics and Trajectory Analysis

During the re-entry, the space vehicle encounters various velocity conditions ranging from hypersonic to subsonic. In the hypersonic and supersonic flight regimes, aerodynamic characteristics of the geometry were determined using the modified Newtonian flow [3], and in the subsonic flight regime, Digital DATCOM was used [8]. The modified Newtonian flow calculated the pressure coefficient $C_p$ of

the windward about free-stream. The leeward side of the body (shadow part of Fig 2.) $C_p$ is set 0. The modified Newtonian flow formula was used as in Eq. 1 [3].

$$C_p = C_{p,max}\sin^2\theta \tag{1}$$

The determination of the angle between the direction of free stream velocity and the surface of the geometry is necessary for the modified Newtonian flow. This angle can be computed using Eq. 2 [3]. This equation involves the normal vector $\boldsymbol{n}$ for each local surface and the free stream velocity vector $\boldsymbol{V}_\infty$.

$$\theta = \frac{\pi}{2} - \cos^{-1}\left(\frac{V_\infty \cdot \boldsymbol{n}}{|V_\infty||\boldsymbol{n}|}\right) \tag{2}$$

To calculate $C_{p,max}$ from Eq. 1, the following Eq. 3 was used. In Eq. 3, $\gamma$ refers to the specific heat ratio and is assumed to be a value of 1.4 under the ideal gas condition.

$$C_{p,max} = \frac{2}{\gamma V_\infty^2}\left[\left\{\frac{(\gamma+1)^2 V_\infty^2}{4\gamma V_\infty^2 - 2(\gamma-1)}\right\}^{\gamma(\gamma+1)}\left\{\frac{1-\gamma+2\gamma V_\infty^2}{\gamma+1}\right\} - 1\right] \tag{3}$$

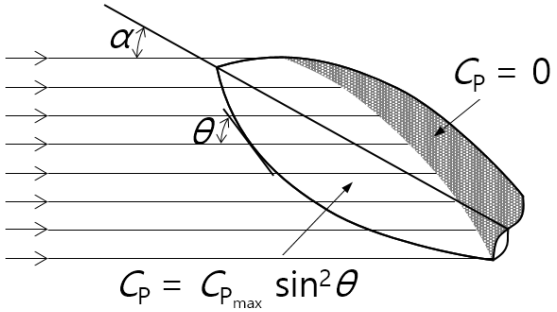


**Fig 2.** Modified Newtonian

For calculating the trajectory during the re-entry, a three-degree-of-freedom (3-DOF) trajectory analysis was employed, incorporating the weight and aerodynamic forces acting on the geometry. The gravity and aerodynamic force at the current position were used to calculate the next position and velocity and then calculate the aerodynamic forces at the next position. At this calculation, the $4^{th}$ Runge-Kutta method was used for time integral, as follows, and X includes velocity and position. The trajectory initial conditions set an altitude of 300km, a velocity of 7,000m/s, and an incline angle of 80°.

$$\dot{X}^{(1)} = f(X^n, t) \tag{4-a}$$

$$\dot{X}^{(2)} = f\left(X^n + 0.5\Delta t\dot{X}^{(1)}, t + 0.5\Delta t\right) \tag{4-b}$$

$$\dot{X}^{(3)} = f(X^n + 0.5\Delta t\dot{X}^{(2)}, t + 0.5\Delta t) \tag{4-c}$$

$$\dot{X}^{(4)} = f(X^n + 0.5\Delta t\dot{X}^{(3)}, t + \Delta t) \tag{4-d}$$

$$X^{n+1} = X^n + \frac{\Delta t(\dot{X}^{(1)} + 2\dot{X}^{(2)} + 2\dot{X}^{(3)} + \dot{X}^{(4)})}{6} \tag{4}$$

### 2.3. Thermodynamic methodology

At hypersonic and supersonic regimes, heat is generated by friction between the air and the geometry's surface. To calculate the heat generation at hypersonic and supersonic regimes, Cohen's method was used to compute at the stagnation point and the approximate convective-heating equation was used excluding the stagnation point [4]. Cohen's method for computing the stagnation point's heat flux is denoted by Eq. 5. Additionally, Eq. 6 is used for calculating the gradient of the velocity of Cohen's method proposed by DeJarnette et al. [10]. The calculation conditions were under the ideal and calorically perfect gas with the Prandtl number 0.71. Viscosity is calculated using Sutherland's equation. The enthalpy of wall and stagnation points are determined by multiplying specific heat at constant pressure and temperature. The density and stagnation point temperature are calculated by normal shock relations [11].

$$\dot{q} = 0.767(Pr_w^{-0.6}) * (\rho_e \mu_e)^{0.5} * \left(h_{stag} - h_w\right) * \sqrt{\frac{du_e}{dx}} \tag{5}$$

$$\frac{du_e}{dx} = \frac{V_\infty}{R} * \sqrt{\frac{1.85\ \rho_\infty}{\rho_{stag}}} \tag{6}$$

The approximate convective-heating equation, excluding the stagnation point, requires inviscid surface streamlines for computation as follows Eq. 8. To generate streamlines, streamline seeds were created at the rear of the geometry and the trailing edge of the wings. Based on the created streamline seeds, streamlines were traced to the stagnation point on the geometry surface, and heat flux was calculated along each streamline. To calculate the streamlines, select the candidate point from the seeds of the streamline in the opposite direction of the surface velocity, calculated Eq. 7. If the candidate point and current point are in the same grid, the candidate point replaces the current point. However, if the candidate point is not placed in the same grid, the candidate point is projected onto the plane which contains other grids [12].

$$\frac{V}{|V|} = \frac{n \times V_\infty \times n}{|n \times V_\infty \times n|} \tag{7}$$

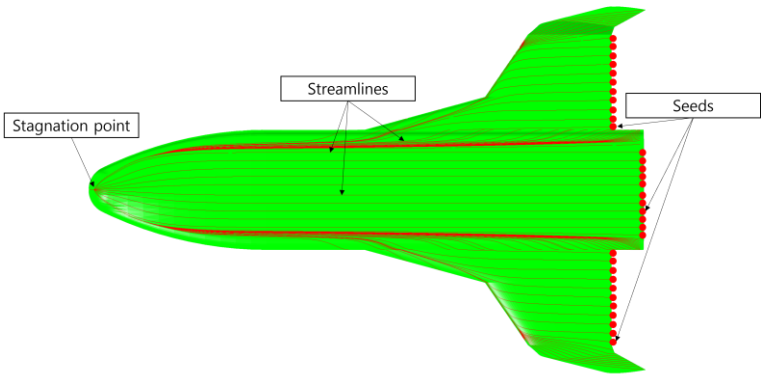


**Fig 3.** Streamline and Seeds

To consider the compressible effect on the hypersonic and supersonic regimes, Eckert's reference enthalpy relation was used which indicates superscript * in Eq. 8 and Eq. 9. Eq. 9 is the calculation of laminar momentum thickness $\Theta_L$. For correction $\Theta_L$, Eq. 10 was used to consider the velocity gradient on the laminar heating proposed by Kemp et al [9]. In Eq. 10, $\bar{\psi}$ denotes the velocity gradient and calculates using Eq. 11. The parameter $\xi$ is determined by the Lees-Dorodnisyn transformation and calculated using Eq. 12 [9].

$$\dot{q_{w,L}} = 0.22(Re_{\Theta_L,e})^{-1}(Pr^{-0.6})(\frac{\rho^*}{\rho_e})(\frac{\mu^*}{\mu_e})\rho_e \mu_e (H_{aw} - H_w) \tag{8}$$

$$\Theta_L = 0.664(\int_0^s \rho^* \mu^* u_e h^2)^{0.5} / (\rho_e \mu_e h) \tag{9}$$

$$\overline{\Theta_L} = \frac{\Theta_L}{1+0.09\sqrt{\bar{\Psi}}} \tag{10}$$

$$\bar{\psi} = \frac{2\xi}{u_e}\left[(\frac{du_e}{ds})/(\frac{d\xi}{ds})\right] \tag{11}$$

$$\xi = \int_0^s \rho_s \mu_w u_e h^2 ds \tag{12}$$

In Eq. 5 and 8, heat flux was calculated as the difference between a wall enthalpy and another enthalpy. To take into account the increased wall temperature caused by aeroheating, wall temperature was calculated using Eq. 13 [13].

$$\dot{q} = \varepsilon \sigma T_w^4 \tag{13}$$

After first calculating the heat flux and wall temperature, the heat flux for the calculated wall temperature is iteratively calculated. Iterative calculation continues until the difference between the existing heat flux and newly calculated heat flux is within 5% (approximately 1% difference in wall temperature). Since, the approximate convective-heating equation was calculated according to the streamline, heat flux calculation for plane that did not intersect the streamline is performed through interpolation. During the re-entry, the maximum heat flux at each surface was recorded for the design

of the Thermal Protection Systems (TPS) layout. The types of TPS used were Felt Reusable Surface Insulation (FRSI), Low-temperature Reusable Surface Insulation (LRSI), High-temperature Reusable Surface Insulation (HRSI), and Reinforced carbon-carbon (RCC). Table 2. presents the characteristics of TPS which used to design the TPS layout.

**Table 2.** Characteristics of TPS type

| TPS type | Temperature range | Areal Density ($kg/m^2$) |
|---|---|---|
| FRSI | Under 644K | 1.6 |
| LRSI | 644K to 922K | 3.98 |
| HRSI | 922K to 1533K | 9.2 |
| RCC | Over 1533K | 44.7 |

### 2.4. Optimization Method

For the multidisciplinary optimization process, a Multi-Objective Genetic Algorithm (MOGA) was conducted with 2 objective functions, 7 constraints, and a design space set of 22 design parameters as outlined in Table 1. The objective functions involve the minimization of weight and standard deviation of heat flux. Minimizing weight aims to reduce the payload of the launch vehicle and the minimization of the standard deviation of heat flux aims to decrease heat flux on the geometry. If reducing the maximum heat flux were set as an objective function, the effect of reducing the heat flux would primarily occur at the stagnation point or leading edge of wings, where the maximum heat flux occurs. However, selecting the minimization of the standard deviation of heat flux allows for considering the effect of reducing heat flux over a large area. The constraints involve unrealistic geometry, maximum dynamic pressure, maximum heat flux, landing speed, trim condition, longitudinal stability, and geometry constraints. The unrealistic geometry refers to examples where the length of the nose is longer than the length of the fuselage, the wings' location behind the fuselage. The constraints include a maximum dynamic pressure set below 50kPa, a maximum heat flux set below 4MW/$m^2$, and a landing speed set below 20m/s. The process of MOGA is depicted in Fig. 4, running with 256 individuals for 100 generations. After 100 generations, the design space is updated with feasible solutions obtained in the last 20 generations.

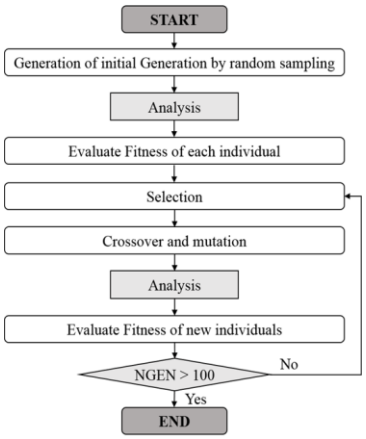


**Fig 4.** MOGA Flow Chart

## 3. Result

Fig. 5 illustrates the baseline shape, KSP-1, provided by KARI. Fig. 7 illustrates the optimized shape, and Table 3 presents the optimization result data. For selecting the weight, the standard deviation of heat flux, and the compromised result, draw a Pareto line with Pareto solutions about objective functions. Due to heat flux affecting the weight, the trade-off relationship is observed in Fig. 6.

**Fig 5.** Baseline Geometry

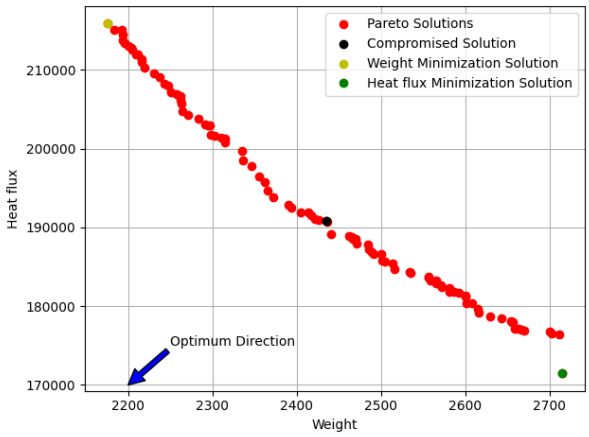


**Fig 6.** Pareto Solutions and Optimum Solutions

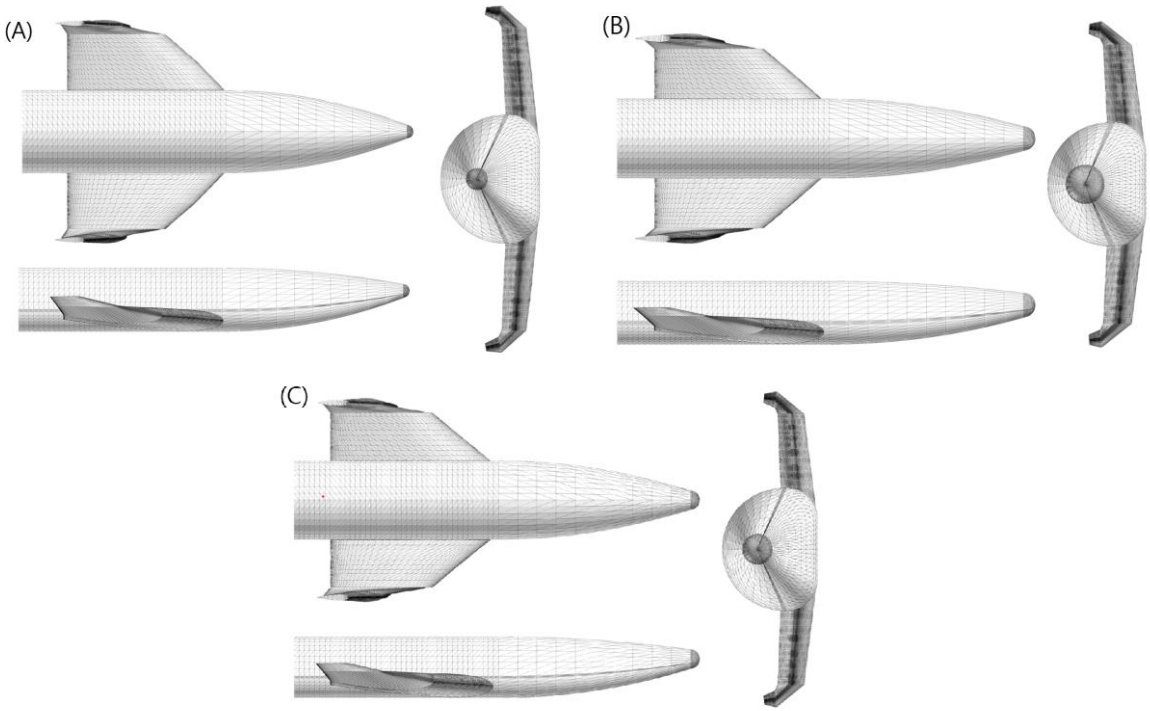

**Fig 7.** Geometries of Optimization Result

A : Weight Minimization Result

B : Heat Flux Minimization Result

C : Compromised Solution Result

**Table 3.** The objective functions comparison

| | Baseline shape | Weight Minimization | Heat flux Minimization | Compromised |
|---|---|---|---|---|
| Weight (kg) | 2,310.36 | 2,175.70 | 2,714.71 | 2,434.59 |
| Heat flux ($W/m^2$) | 335,314.40 | 215,864.63 | 171,471.48 | 190,836.89 |

The previous TPS layout was determined based on geometry. However, in this study, the TPS layout was modified based on wall temperature. Table 4. presents a comparison of the two methods.

**Table 4.** Comparison of geometry-based and wall temperature-based TPS layout weight

| Weight (kg) | Weight Minimization | Heat flux minimization | Compromised |
|---|---|---|---|
| Geometry based | 2,384.36 | 2,960.55 | 2,636.82 |
| Temperature based | 2,175.40 | 2,714.71 | 2,434.59 |

Fig. 8 illustrates the comparison of the TPS layout at the bottom of the geometry between the two methods. The dark gray color represents RCC, the gray and light gray color denotes HRSI, and LRSI, and the brown color indicates FRSI. At the stagnation point and the leading edge of the wings, both RCC is coated. However, when the TPS layout is designed with wall temperature, it can be observed that the RCC area is positioned where the curvature is formed by the bottom of the fuselage where the geometry-based TPS layout cannot protect from the high temperature.

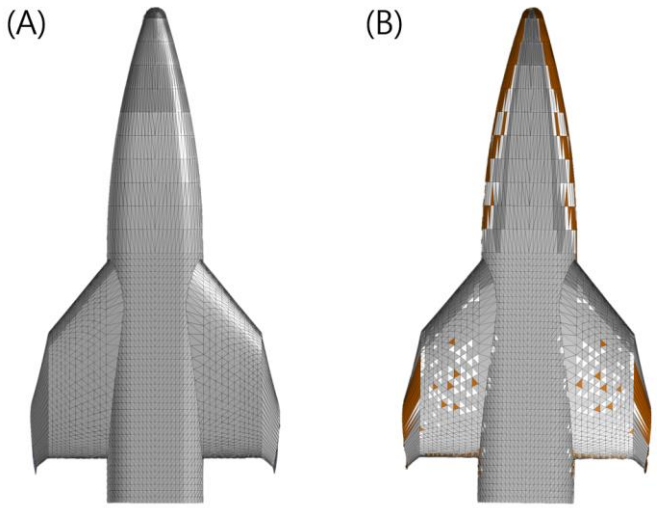


**Fig 8.** Comparison of TPS Layout

A : Geometry-Based TPS Layout

B : Wall Temperature-Based TPS Layout

## 4. Conclusion

A multidisciplinary optimization with a wall temperature-based TPS layout has been examined for minimizing the space vehicle's weight and standard deviation of heat flux. Compared with a geometry-based TPS layout, the weight was lower at each optimal point. In addition, the safety of the space vehicle can be secured in high-temperature areas that are not considered in the geometry-based TPS layout.

## Acknowledgment

This work was supported by the Korea Research Institute for Defense Technology Planning and Advancement (KRIT) grant funded by the Korean government (DAPA) (No. KRIT-CT-22-030, Reusable Unmanned Space Vehicle Research Center)

## References

1. David W. W., Kenneth D. M., Frank O., Apollo 11 Day 9, part 2: Entry and Splashdown. https://history.nasa.gov/afj/ap11fj/27day9-entry.html. Accessed 12 October 2023
2. Timothy T. AS., Lain D. B., Lian D., Junji H.: Assessment of Reynolds Average Navier-Stokes Models for a Hypersonic Cold-Wall Turbulent Boundary Layer, AIAA SciTech Forum, AIAA. 2022.
3. John, D. Anderson Jr.: Hypersonic and High-Temperature Gas Dynamics. AIAA Education Series (2019)
4. E. V. Zoby., J. N. Moss., K. Sutton.: Approximate Convective-Heating Equations for Hypersonic Flows. Journal of Spacecraft and Rockets. AIAA. 18, 64-70 (1981)
5. Murata, T., Ishibuchi H.: MOGA: multi-objective genetic algorithms. IEEE international conference on evolutionary computation. IEEE. Vol. 1, 289-294 (1995)
6. Jongho Jung.: Development of an Efficient Multidisciplinary Optimization Method for the Conceptual Design of Reusable Unmanned Spacecraft. Dissertation, Seoul National University, (2023)
7. Harloff, G. J., Berkowitz, B. M.: HASA-Hypersonic Aerospace Sizing Analysis for the Preliminary Design of Aerospace Vehicles. Cleveland. Ohio. USA (1998)
8. Williams, J. E., Murray, S. C., Mehlick, G. J., Sellers, T. B.: The USAF Stability and Control Digital Datcom Volume 1: Users Manual. St. Louis, Missouri, USA, (1979)
9. Kemp N. H., Rose P. H., Detra R. W.: Laminar heat transfer around blunt bodies in dissociated air. Journal of the Aerospace Sciences. AIAA. 26, 421-430 (1959)
10. DeJarnette F. R., Hamilton H. H., Weilmuenster K. J., Cheatwood F. M.: A review of some approximate methods used in aerodynamic heating analyses. Journal of Thermophysics and Heat Transfer. AIAA. 1, 5-12 (1987)
11. John, D, Anderson Jr.: Modern Compressible Flow With Historical Perspective. McGraw-Hill, New York (2004)
12. Lo, S. H.: Automatic Mesh Generation over Intersecting Surfaces. International Journal for Numerical Methods in Engineering. Vol. 38, No. 6, 943-954 (1995)
13. Bertin, J. J.: Hypersonic Aerothermodynamics. AIAA Education Series (1994)